Model-based displacement estimation of wind turbine blades using strain modal data

Model-based displacement estimation of wind turbine blades using strain modal data

J Gundlach[1], J Knebusch[1], Y Govers[1] and B Haller[2]

[1] German Aerospace Center (DLR), Institute of Aeroelasticity, Bunsenstraße 10, 37073 Göttingen, Germany.
[2] Fraunhofer Institute for Wind Energy Systems (IWES), Am Seedeich 45, 27572 Bremerhaven, Germany.

E-mail: janto.gundlach@dlr.de

Abstract. For wind turbine rotor blades, the use of strain sensors is preferred over acceleration sensors for the purpose of permanent monitoring. Experimental modal analysis during operation is thus constrained to strain information, yielding strain modal data including strain mode shapes. For follow-up investigations such as aerodynamic load assessment or flutter monitoring it is however advantageous to have this information as displacement mode shapes or as displacements of the blade contour over time. This research applies a generic approach that converts strain mode shapes to displacement mode shapes utilizing an FE shell model as a basis for approximation. The accuracy of the approach is assessed by comparison with experimentally identified high-resolution displacement mode shapes which are acquired with accelerometers and serve as a reference. In the process the conversion procedure is illustrated with the help of strain data that has been obtained using a sensor instrumentation installed for certification testing of the blade. The requirements for successful usage of the employed conversion scheme and its suitability for rotor blade data are discussed.

1. Introduction

In certain applications of aerospace and wind turbine technology, structural responses are prevalently measured using strain sensors. As part of the certification process of newly developed rotor blades, strain data is recorded for internal stress analysis during static and high cycle fatigue testing for the purpose of design validation. During operation, strain gauges are likely to be used for monitoring the blade deformation, and continuous progress in fiber optical sensing seems promising for future use of these technologies.

With regard to the dynamic behavior of wind turbine rotor blades, response signals can be employed to identify strain mode shapes describing the deformation of the structure when being excited at its natural frequencies [1]. By means of monitoring, these modal properties are subjected to changes due to varying operational and environmental conditions, and setting up numerical models for the whole envelope of operational states is a costly task. Since rotor blade certification does not require rigorous modal testing in terms of detailed eigenforms, the validation of FE rotor blade models is constrained when it comes to the predictive capability of dynamic deflections. Imprecise prediction of the displacement eigenbehavior may then result in a flawed prognosis on the overall loading of the wind turbine or erroneous assessment of stability

problems such as flutter. For this reason, reliable strain to displacement conversion techniques which work on real-time data could be a valuable contribution in wind turbine technology.
Different techniques have been proposed for the purpose of converting strain measurements to displacement estimates. In some cases it is directly possible to exploit the kinematics which have been derived for simplified mechanical structures like beams [2, 3]. Although rotor blades are often modeled using beam elements, the simplification implies neglecting various physical phenomena like cross-sectional vibrations which have become more important for modern blades. Several more generic approaches are based on modal transformation to construct the displacement-strain relation [4, 5]. For the modal expansion it is important to include all relevant modes that contribute to the response and the quality of approximated modal coordinates depends on the number and distribution of the strain sensors. Apart from measured strain data, such approaches necessitate both reliable strain mode shapes and displacement mode shapes coming from an FE model. In [6] a conversion scheme is presented which is supposed to yield promising results of displacement mode shapes and displacement responses even if the eigenforms from the FE model do not match perfectly with the actual behavior of the structure. The method is based on experimentally identified strain mode shapes which are utilized for approximation by a linear combination of a subset of FE strain mode shapes. In doing so, the experimental mode shape is distributed on several numerical mode shapes instead of a one-on-one correlation. The composition of the subset is determined by the so-called local correspondence principle introduced in [7], and the coefficients of the linear combination are used to give an estimate on displacement mode shapes.
In this research the scheme illustrated in [6] will be applied on strain measurements acquired in dynamic tests of a 20 m demo scale wind turbine blade to estimate displacement data. The rotor blade was manufactured by DLR with a geometric bend-twist coupling for passive load reduction [8]. It exhibits coupled mode shapes and is thus well-suited to verify the method for complex-shaped blade designs. The conversion is carried out with the help of an FE shell model that was designed directly from the production drawings [9, 10]. Estimated displacement mode shapes are then compared to experimental high-resolution displacement mode shapes which are acquired with accelerometers and serve as reference.
The displacement mode shapes have been obtained in the same measurement campaign presented in [11]. In contrast to the previous report, section 2 provides insight in the test procedure for identifying strain modal data. The details of the test instrumentation are elucidated and the applied techniques of experimental modal analysis are explained briefly. Furthermore, a variety of results of the modal properties of the blade are shown. Section 3 summarizes the theoretical framework of the conversion algorithm and illustrates its application on the modal strain data of the rotor blade. In section 4 the estimated and experimentally identified displacement data is compared and the applicability of the method is discussed, before the recent findings of this paper are concluded in section 5.

2. Identification of strain modal parameters

The rotor blade has been tested being clamped to a test rig at Fraunhofer Institute for Wind Energy Systems (IWES) in Bremerhaven, Germany. Modal characterization has been conducted subsequent to static extreme load tests but before fatigue testing. To achieve a decent response of the structure, slow-paced logarithmic sine up-sweeps in the range of 1-64 Hz have been performed. The excitation has been accomplished incorporating an electrodynamic long stroke shaker with ± 7.5 cm of travel. The measurement range is divided in a lower frequency band from 1-5 Hz where the shaker is in rigid supports and a higher frequency band in which the shaker is seismically supported in suspensions. In the following an overview of the test scenario is provided and the derivation of modal parameters is explained.

2.1. Measurement setup and instrumentation

The measurement installation represents the equipment which has also been used in the static and fatigue load tests for the certification of the blade. In total 151 signals coming from strain gauges have been recorded. A subset of 117 sensors measuring in 0° and 90° with respect to the blade length axis is used for experimental modal analysis.

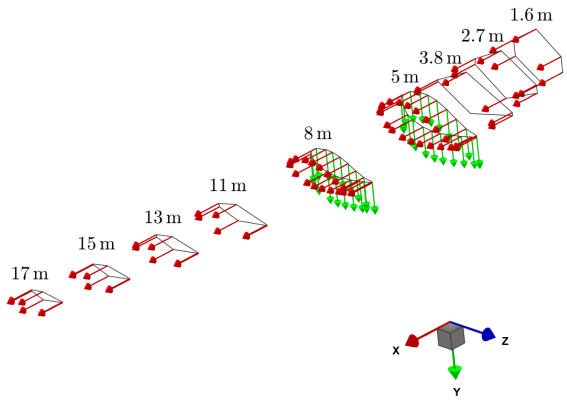

Figure 1: Distribution of employed strain gauges for modal analysis.

With regard to blade certification [12], strain gauges are the common way to determine the reached bending moment distribution especially during the fatigue test. For this purpose, the calibration of the strain gauge values to induced bending moments is carried out. The sensors are supposed to be distributed on the main load carrying structure e.g. spar cap in upper and lower shell at a minimum of 4 cross sections. Other locations of interest are sections with maximum chord length from the leading to the trailing edge of the blade and the transition area from the circular root profile to the actual airfoil. Typically solely sensors measuring in longitudinal direction are used.

In Fig. 1 the location of considered strain gauges is visualized. As depicted, strains are measured in 9 radial positions along the rotor blade. In every section red arrows denote sensors measuring in length direction, whereas in only 2 sections arrows pointing in y-direction assign sensors that measure strains in-plane with the blade surface, but orthogonal to the length direction. Even by dismissing available strain gauges measuring in $\pm 45°$ and sensors located on the shear web, the sensor density is significantly higher compared to the usual installation setup according to the testing guideline.

2.2. Experimental strain modal analysis of the rotor blade

From a theoretical stand point strain modal analysis in the frequency domain has several similarities with classical experimental modal analysis (EMA) incorporating accelerometers. During the test, the blade is excited by a known force while strain sensors are measuring the deformation response. The time signals of the excitation and the strain response are utilized to estimate strain frequency response functions (FRFs) using the same estimators that would also apply for accelerations. Measured strain FRFs are then the basis for identification methods to extract the modal parameters. There are differences between experimental strain and displacement modal analysis concerning mainly the properties of the FRF matrix that impede the mass-normalization of mode shapes [13], which is irrelevant for present investigations.
Since two different measurement systems have been employed to record the force cell and the strain gauges, respectively, the strain response signals must be time synchronized with the excitation force. This is accomplished by finding the maximum of the cross-correlation function of a reference signal which was measured simultaneously on both machines. The location of the maximum in the time series corresponds to the time delay.

In Fig. 2(a) the collected time data of all considered strain sensors during a flapwise sine up-sweep is displayed. With the force amplitude set to constantly 580 N, strain responses up to 300 μm/m are obtained. The sweep corresponds to the frequency band where the electrodynamic shaker is seismically supported in suspensions. Thus, the first elevation which is observed in the

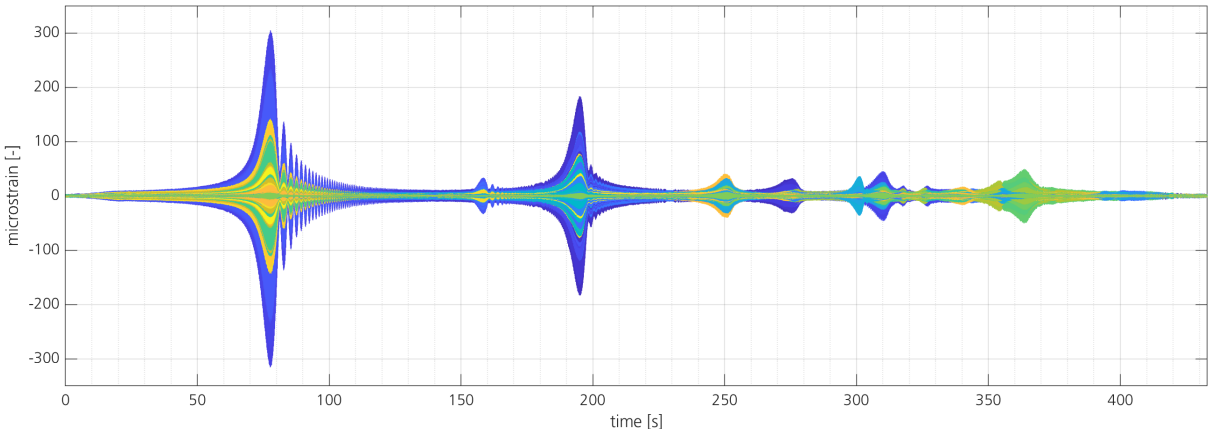

(a) Recorded strain response signals.

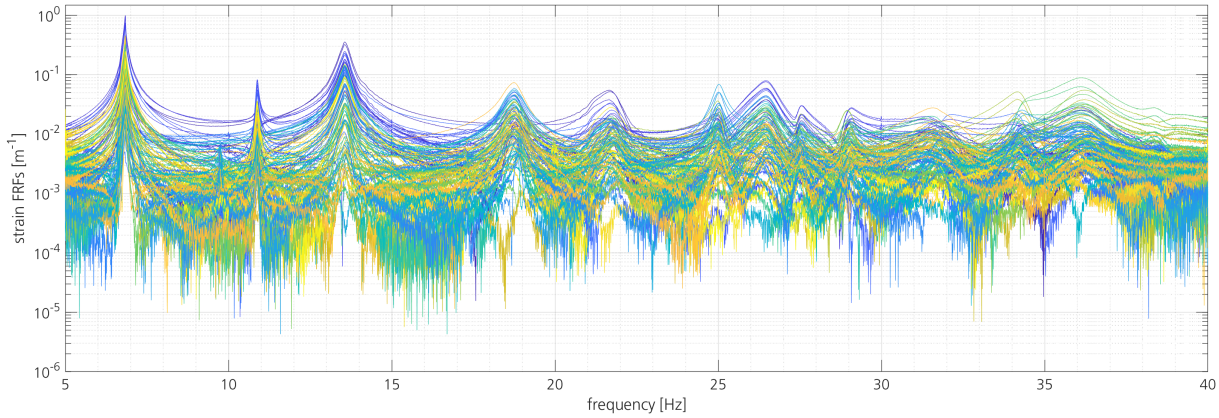

(b) Corresponding strain FRFs in the frequency band up to 40 Hz.

Figure 2: Time and frequency data obtained from a sine up-sweep of 0.5 oct/min in a frequency range from 5 Hz to 64 Hz.

time series occurs when the excitation signal passes the eigenfrequency of 2$^{\text{nd}}$ bending flapwise (cf. Tab. 1). For this study, response signals have only been recorded from flapwise excitation runs, but attributed to the high force level each mode is supposed to be sufficiently excited in terms of the signal-to-noise ratio of common strain gauges.
The acquired time data is processed to strain frequency response functions using Welch's method to approximate the involved spectra. The magnitudes of all strain FRFs are displayed for the corresponding time series in Fig. 2(b). They are the starting point of the PolyMAX algorithm as described in [14] which identifies the modal parameters i.e. eigenfrequencies, modal damping, and eigenforms of the rotor blade.
An overview of the identification results is displayed in Tab. 1. Regarding identified eigenfrequencies the EMA approaches lead to very similar values. Differences in the lower frequency range are to the size of the frequency resolution of the spectra. For higher modes, discrepancies may also be caused due to different excitation techniques and force levels as applied in the displacement EMA (cf. section 4). The FE model consists mainly of linear CQUAD4 elements and contains concentrated masses accounting for the sensor instrumentation on the blade. The eigenvalue analysis is performed using MSC.Nastran. With increasing modes, the model tends to predict lower eigenfrequencies with the largest deviation on the 1$^{\text{st}}$ torsion mode. For the last two modes there is no sufficient one-on-one correlation. This becomes apparent in Fig. 3 where

identified strain mode shapes are compared to predicted shapes from FE analysis in terms of the modal assurance criterion (MAC). In order to evaluate the corresponding strain for each sensor position from the model, the strain values at FE nodes closest to the actual measurement positions are utilized. Since a single node is part of all adjacent finite elements, several extrapolated strain values are available at one grid point. On that account, the arithmetic mean of these values is used. The MAC matrix indicates the tendency of sound agreement for lower modes with decreasing correlation for higher frequencies. In particular the mode shape of 1st torsion exhibits a rather poor correlation with the model.
It should be noted that the listed modes represent only a selection of global mode shapes which are typical for rotor blades of wind turbines. Additional modes have been identified in both displacement EMA (cf. [11]) and strain EMA yielding cross-sectional breathing of the rotor blades. Unfortunately, these modes do not correlate with the existing FE model, hence they are excluded for the purpose of this research.

Table 1: Eigenfrequencies of the 20 m demo blade: results from EMA and FEM prediction.

	f in Hz		
description	classical EMA	strain EMA	FEM
1st flapwise	2.20	2.20	2.23
1st edgewise	3.07	3.07	2.95
2nd flapwise	6.84	6.83	6.66
2nd edgewise	10.86	10.88	9.83
3rd flapwise	13.57	13.59	12.72
1st torsion	18.78	18.70	14.60
4th flapwise	21.65	21.75	19.39
3rd edgewise	26.49	26.51	24.80
5th flapwise	28.78	28.91	-
2nd torsion	31.50	31.65	-

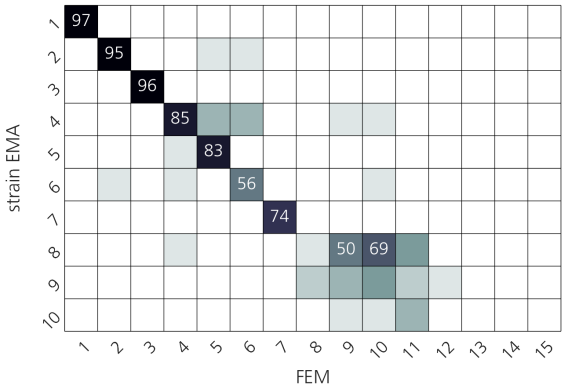

Figure 3: MAC matrix of strain EMA mode shapes vs. FEM prediction.

In order to get an impression of the actual shape of strain eigenforms, a selection of strain mode shapes is illustrated in Fig. 4. Rather simple eigenforms like the 1st flapwise bending mode are plausible on the first glance; i.e. areas that are stretched in length direction of the blade are simultaneously compressed in the pependicular direction and vice versa. For more complicated eigenforms such as the 1st torsion mode the interpretation of the deformation is certainly cumbersome compared to displacement mode shapes.

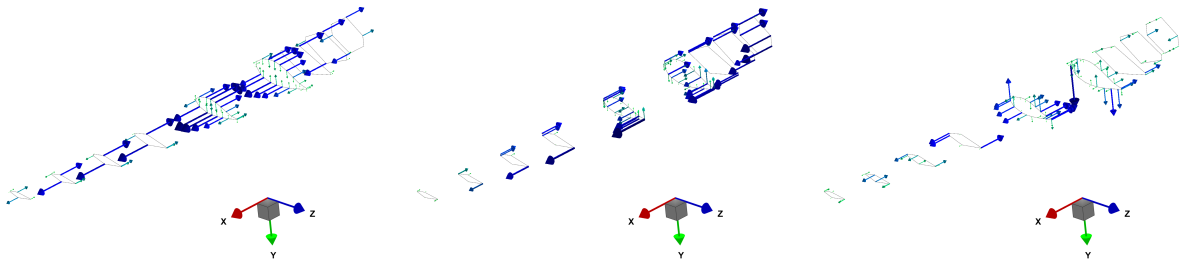

(a) 2.2 Hz (b) 3.1 Hz (c) 18.7 Hz

Figure 4: Choice of strain mode shapes: 1st flapwise (a), 1st edgewise (b), and 1st torsion (c). Arrows pointing in positive coordinate directions represent elongations. Arrows aligned with the y-coordinate direction illustrate strains that occur in-plane with the surface, perpendicular to the x-direction.

3. Strain to displacement conversion scheme

After having correlated the test results with predictions obtained by the FE model, the conversion is carried out as follows. The approach proposed by [6] assumes that every experimental strain mode shape $\boldsymbol{\psi}^x$ can be represented by a linear combination of FE strain mode shapes:

$$\boldsymbol{\psi}^x = \boldsymbol{\Psi}_m^{fe} \boldsymbol{p}_m. \tag{1}$$

In this equation the matrix $\boldsymbol{\Psi}_m^{fe}$ represents a subset of m FE strain mode shapes and $\boldsymbol{p}_m$ specifies the corresponding coefficients of the linear combination. An approximation

$$\hat{\boldsymbol{p}}_m = \boldsymbol{\Psi}_m^{fe\dagger} \boldsymbol{\psi}^x \tag{2}$$

of the coefficients can be determined using least squares with $\boldsymbol{\Psi}_m^{fe\dagger}$ being the pseudo inverse of the subset. If linearity applies to the structure, Eq.(1) holds also for a displacement mode shape $\boldsymbol{\phi}^x$ such that an estimate is found in

$$\hat{\boldsymbol{\phi}}_m^x = \boldsymbol{\Phi}_m^{fe} \hat{\boldsymbol{p}}_m, \tag{3}$$

where $\boldsymbol{\Phi}_m^{fe}$ denotes the displacement equivalent of $\boldsymbol{\Psi}_m^{fe}$. The ideal choice of FE mode shapes serving as a subset for the approximation is determined by the so-called principle of local correspondence [7], which is illustrated for the present application in the following subsections.

3.1. Selection of appropriate FE mode subset

The local correspondence principle can be derived from sensitivity analysis of mode shapes as described in [15]. Given that discrepancies between experimental and numerical mode shapes are attributed to perturbations of the mass or stiffness matrix, the principle allows the approximation of a specific experimental (perturbed) mode shape using the corresponding numerical (unperturbed) mode shape and a limited number of numerical modes around (in terms of frequency) it. For each individual mode shape which is subjected to approximation, a ranking of FE strain modes is compiled, starting with the mode shape of highest MAC value and followed by modes with increasing frequency deviation to the mode of interest.

The ranking defines the order of which FE mode shapes will be included in $\boldsymbol{\Psi}_m^{fe}$ as columns, but there is a rule required to decide on the number of mode shapes to be used. In the present work the procedure suggested by [7] is employed, where the error at un-fitted degrees of freedom (DOFs) is used as a quality measure for the approximation. In the process approximated mode shapes are separated on sets of fitting and observation DOFs:

$$\hat{\boldsymbol{\psi}}_m^x = \begin{bmatrix} \hat{\boldsymbol{\psi}}_{fit,m}^x \\ \hat{\boldsymbol{\psi}}_{obs,m}^x \end{bmatrix} = \begin{bmatrix} \boldsymbol{\Psi}_{fit,m}^{fe} \\ \boldsymbol{\Psi}_{obs,m}^{fe} \end{bmatrix} \hat{\boldsymbol{p}}_m. \tag{4}$$

In above expression $\boldsymbol{\Psi}_{fit,m}^{fe}$ and $\boldsymbol{\Psi}_{obs,m}^{fe}$ represent subsets of FE strain mode shapes distributed on fitting and observation DOFs, respectively, and in contrast to Eq.(2), the coefficients of the linear combination are estimated by

$$\hat{\boldsymbol{p}}_m = \left(\boldsymbol{\Psi}_{fit,m}^{fe} \right)^{\dagger} \boldsymbol{\psi}_{fit}^x \tag{5}$$

using the experimental strain mode shape defined on fitting DOFs solely. The quality of the approximation based on m modes in the subset is assessed by means of the MAC value between the observation estimate and the corresponding experimentally identified mode shape:

$$\gamma(m) = \mathrm{MAC}\left(\hat{\boldsymbol{\psi}}_{obs,m}^x, \boldsymbol{\psi}_{obs,m}^x \right). \tag{6}$$

In doing so, the approximation results at the observation DOFs are applied as test data for coefficients trained by FE mode shape values at the DOFs used in the fitting. The quality measure γ exhibits a maximum if a certain number m_o of FE modes is considered in the subset. In case of fewer modes, the approximation result could be improved according to the local correspondence principle, whereas upwards of m_o the experimental mode shape is over fitted. Obviously, the results obtained in Eq.(6) for an optimal subset will strongly depend on the definition of DOFs for fitting and observation purpose as displayed in Eq.(4). In order to avoid possible error which may occur due to an inappropriate division, the finding of the optimal number of FE modes is accomplished in a repetitive loop with all but a single DOF being used for the fitting, while the DOF of observation is roved over all measurement DOFs. That way each cycle of the loop contributes with a single component to $\hat{\boldsymbol{\psi}}^{x}_{obs,m}$, before the approximation is evaluated in Eq.(6) over the entirety of DOFs.
After m_o is found, the optimal coefficients can be determined using Eq.(2) over the full set of measurement DOFs and the approximated displacement mode shape is computable with the help of FE displacement mode shapes through Eq.(3).

3.2. Applying the approach on rotor blade strain data

The outlined procedure is applied to the experimentally identified strain mode shapes. With regard to the correlation matrix (cf. Fig. 3), the selection of not more than 15 modes from FE calculation seems adequate as basis for the mode shape approximation. In Fig. 5 the estimated coefficient of the linear combination according to Eq.(2) are shown for each individual mode. The number of eigenforms which are included in the subset varies between 6 and 14 modes. The FE modes appear in the subset as defined by the unique ranking provided by the local correspondence principle. Naturally, the contribution coming from the first ranked vector is for all mode shape approximations the largest. Furthermore, eigenforms with low or none one-on-one correlation, such as the 1st and 2nd torsion mode, tend to obtain higher contributions from modes further away from their own eigenfrequency.

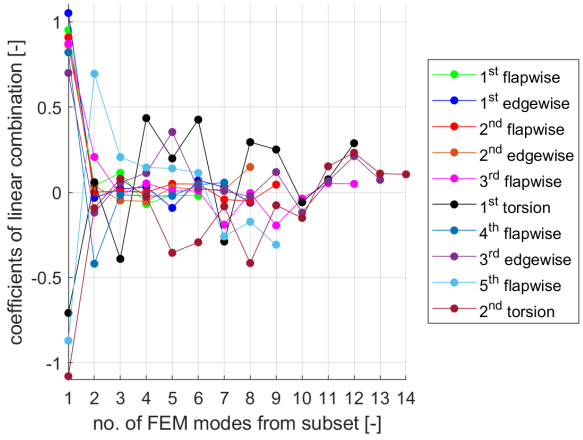

Figure 5: Coefficients of linear combination $\hat{\boldsymbol{p}}_m$ of all approximated mode shapes.

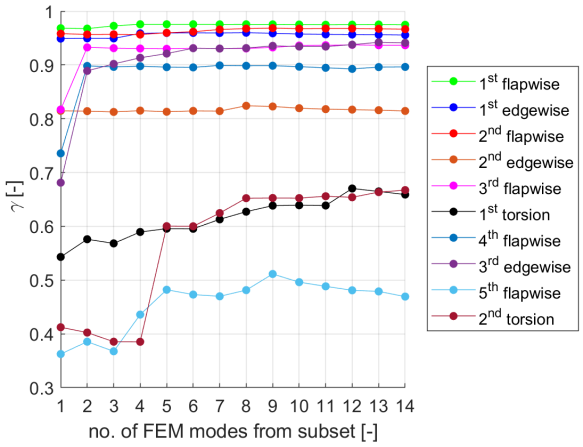

Figure 6: Qualitiy measure $\gamma(m)$ vs. number of modes included in the approximation.

The quality measure of the approximation by means of Eq.(6) is plotted in Fig. 6 for different amounts of mode shapes in the subset. In case of modes that show high one-on-one correlation, the potential for possible changes is rather low compared to those modes which start significantly lower. The number of modes which corresponds to the maximum value is used as optimal choice with avoidence of overfitting.

With the help of the approximated coefficients an estimate for all strain mode shapes is compiled and compared to the actual identified mode set (cf. Fig. 7). In the diagram each identified strain mode shape is technically correlated with a certain number of FE mode shapes which serve as basis for approximation. Although the appearance of the plot seems to be symmetric, the approximated mode shapes do not form symmetric MAC matrices with the test data set. Compared to the one-on-one correlation displayed in Fig. 3 there are notable improvements for every mode except for the 2nd edgewise bending eigenform. The modes that benefit most of the approximation procedure are those which have achieved also the higher gains in Fig. 6; for instance the two torsion modes.

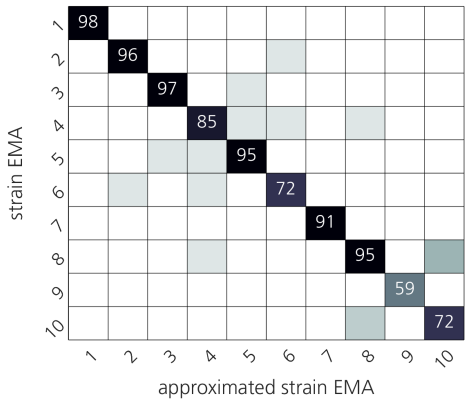

Figure 7: MAC matrix of strain mode shape approximation vs. FEM.

4. Comparison results

Finally, the strain to displacement conversion is carried out according to Eq.(3) and the approximation results are compared to mode shapes identified from classical EMA. Regarding the classical EMA, the instrumentation on the blade consists of 265 uniaxial acceleration sensors which are positioned in 29 sections on the pressure side and in 15 sections on the suction side. Excitation has been accomplished in flapwise and edgewise direction using both single input and multi-point input techniques incorporating up to two electrodynamic shakers which induce either sine-sweep or broadband random forces. The resulting modal model has been derived from various measurement runs and is thus considered as a reliable reference. More detailed information on the whole modal test campaign and the visualization of identified mode shapes is provided in [11].

Figure 8 compares the outcome of the displacement mode shape approximation to the reference data. The approximation considers the equivalent ranking of FE displacement shapes at the respective DOFs of the classical EMA. As seen from the correlation matrix, the scheme produces in general better agreement for flapwise modes compared to edgewise modes. The first and second flapwise mode are resolved well, the same applies to the first bending edgewise. The second edgewise mode and the higher flapwise bending modes are still acceptably met, yet there is no sound matching between the first and second torsion mode to their true eigenform. Also, the 3rd edgewise mode is not successfully reproduced by the scheme, although the calculated linear combination yields a promising 95% in the strain shape approximation (cf. Fig. 3).

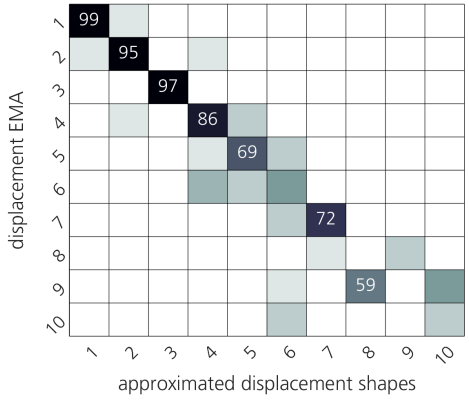

Figure 8: MAC matrix of classical EMA vs. displacement mode shape approximation.

Since the approach necessitates an FE model, the capability of the conversion technique can be assessed in consideration of the classical MAC matrix between the FE model and displacement EMA as illustrated in Fig. 9. At first, this comparison is quite sobering. Apparently the FE model exhibits already a better agreement in displacement eigenform prediction than any of the

approximated mode shapes which are based on an FE mode subset. Hence, the question arises whether the proposed procedure should be prefered over the direct use of the FE prediction. Before this question is answered, possible constraints that might cause the degradation of the quality of the obtained approximation results are discussed. The authors are convinced that the strongest assumption being part of the algorithm is the linearity postulate as formulated in Eq.(3). Although the linear relationship is self-evident in theory, it is however very difficult to meet this condition regarding practical aspects.

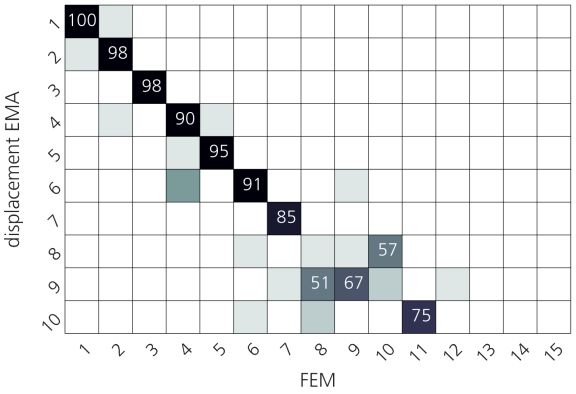

Figure 9: MAC matrix of classical EMA vs. FEM.

Below three domains are exemplified which are likely to impede the linearity assumption. They are also starting point for future research need in this area of investigation:

- *FE discretization*
  In finite element analysis the prediction of accurate strain information is more cumbersome compared to nodal displacements. As mentioned above, plate elements with linear shape functions (CQUAD4) have been used in the eigenvalue analysis. Strain eigenforms are commonly derived in a postprocessing step where a linear differential operator is applied on the displacement deformation. Increasing the order of the shape functions, i.e. using higher order elements may lead to more accurate strain shape predictions. Furthermore, an insufficient resolution of elements is a possible reason for inaccurate strain predictions. Thus, mesh refinement studies could bring more insight.
- *Correlation analysis*
  As described in section 2.2 the strain values for evaluating the modal assurance criterion are taken from the closest neighboring grid point of the strain gauge. The grid point value itself represents only the arithmetic mean of four extrapolated values coming from normally four elements that are connected at that node. In cases of larger distances between the sensor and the grid point this is an additional source of error. For the displacement MAC assessment inaccuracy occurs due to acceleration sensors which are not directly associated to a single grid point. A higher accuracy could be obtained using elaborated interpolation techniques.
- *Strain modal testing*
  In contrast to the classical EMA, strain EMA is only carried out using single-input sine sweeps in flapwise direction. Possibly the adequacy of the strain mode shapes could be improved by analyzing measurement runs coming from different sorts of excitation. This might be especially the case for mode shapes with edgewise and torsional deformations.

If the used sensor instrumentation of displacement EMA and strain EMA was equivalent in effectiveness, the correlation matrices in Fig. 3 and Fig. 9 would yield the very same results, given that linearity holds. The potential of the conversion scheme would then be analog to the improvements observed in Fig. 7. Unfortunately, attributed to above described factors, the exploitation of linearity is flawed such that the result obtained by approximation is worse compared to the one-on-one correlation with FE mode shapes. To utilize the potential of the procedure, the requirements have to bet met carefully beforehand.

5. Summary and conclusions

In this report a model-based strain to displacement conversion approach has been operated on experimentally identified rotor blade modal data. The strain eigenforms applied in the conversion have been determined using the sensor instrumentation installed for rotor blade certification purpose. The conversion results are compared to high-resolution displacement eigenforms derived in the same test campaign. It turns out that successfully employing the conversion technique on rotor blades crystallizes in high demands on strain modal testing, FE model discretization, and correlation analysis between experimental and numerical data. Nevertheless, during operation the momentary eigenbehavior in terms of displacement is commonly unknown and due to external parameter changes the behavior could be out of scope of predictive capability of the FE model. In these cases displacement approximation using real-time strain data still represents a conceivable solution which needs further research.

Acknowledgments

This work was partially funded by the German Federal Ministry for Economic Affairs and Energy (BMWi) in the SmartBlades2 project (0324032A-H). The authors are much obliged to all members of the DLR modal test team and to the on-site support provided by Fraunhofer IWES, Bremerhaven.

References

[1] Di Lorenzo E, Manzato S, Peeters B, Ruffini V, Berring P, Haselbach P U, Branner K and Luzcak M M 2020 *Topics in Modal Analysis & Testing* **8** 143-52
[2] Wang Z, Geng D, Ren W and Liu H 2014 *Smart Mater. Struct.* **23** 125045
[3] Piana G, Lofrano E, Carpinteri A, Paolone A and Ruta G 2016 *Meccanica* **51** 2797-811
[4] Bogert P B, Haugse E and Gehrki R E 2003 *Structural shape identification from experimental strains using a modal transformation technique* (Norfolk, VA: 44th AIAA/ASME/ASCE/AHS/ASC Structures, Structural Dynamics and Materials Conference)
[5] Kang L, Kim D and Han J 2007 *J. Sound Vib.* **305** 534-42
[6] Skafte A, López-Aenlle M and Brincker R 2016 *Smart Mater. Struct.* **25** 025020
[7] Brincker R, Skafte A, López-Aenlle M, Sestieri A, D'Ambrogio W and Canteli A 2014 *Mech. Syst. Signal Process.* **45** 91-104
[8] Montano M, Kühn M, Daniele E and Stüve J 2018 *Lightweight Des. worldw.* **11** 42-7
[9] Willberg C 2020 *Smartblades 2 finite element reference wind turbine blade model* (DOI: 10.5281/zenodo.3628356, available from 08/2020)
[10] Willberg C 2020 *Validation of a 20m wind turbine blade model* (currently under review in *Wind En. Sc.*)
[11] Gundlach J and Govers Y 2019 *J. Phys.: Conf. Ser.* **1356** 012023
[12] Wind turbines - Part 23: Full-scale structural testing of rotor blades 2014 *IEC 61400-23*
[13] Kranjc T, Slavic J and Boltezar M *J. Vib. Control* **20**(2) 371-81
[14] Peeters B, Auweraer H V, Guillaume P and Leuridan J 2004 *Shock and Vibration* **11** 395-409
[15] Heylen W, Lammens S, Sas P 2007 *Modal analysis theory and testing* (Leuven: Katholieke Universiteit Leuven, Faculty of Engineering)